



A Photoionization Reflectron Time-of-flight Mass Spectrometric Study on the Formation of Acetic Acid (CH₃COOH) in Interstellar Analog Ices

Alexandre Bergantini^{1,2} , Cheng Zhu^{1,2} , and Ralf I. Kaiser^{1,2} ¹ Department of Chemistry, University of Hawaii at Mānoa, Honolulu, HI 96822, USA² W. M. Keck Laboratory in Astrochemistry, University of Hawaii at Mānoa, Honolulu, HI 96822, USA; ralfk@hawaii.edu

Received 2018 May 1; revised 2018 June 22; accepted 2018 June 25; published 2018 August 1

Abstract

This work investigates the synthesis of complex organic molecules with special focus on acetic acid (CH₃COOH) via experiments involving the processing of astrophysical model ices of carbon dioxide–methane (CO₂–CH₄) by low doses of ionizing radiation, exposing the initial bond-breaking processes and successive reactions initiated by energetic electrons generated in the track of galactic cosmic-ray particles penetrating ice-coated interstellar grains, deep inside molecular clouds in their early stages of evolution. The key results were obtained through single photoionization reflectron time-of-flight mass spectrometry (PI-ReTOF-MS) and exploiting isotopically labeled samples (C¹⁸O₂–CH₄; CO₂–CD₄). Not only acetic acid (CH₃COOH), along with fragments of acetic acid dimers (CH₃COOH)₂, but also the hitherto elusive interstellar methyl hydroperoxide (CH₃OOH) and the hydrocarbons ethane (C₂H₆) and butane (C₄H₁₀), along with species belonging to C₂H₄O, C₂H₆O, and C₃H₆O₂ isomers, are swiftly formed via suprathermal reactions at doses of only 0.88 ± 0.12 eV per molecule of carbon dioxide and 0.32 ± 0.04 eV per molecule of methane, which is equivalent to doses deposited in just (2.0 ± 0.5) × 10⁶ yr in a typical molecular cloud. The results suggest further that the search for acetic acid dimers (CH₃COOH)₂ toward star-forming regions has a significant potential to be successful. Finally, methyl hydroperoxide (CH₃OOH) and dimethyl peroxide (CH₃OOCH₃), as identified previously in our laboratory, are predicted to be present in the interstellar medium, thus providing a homologous series of peroxides—HOOH, CH₃OOH, and CH₃OOCH₃—to shed light on the interstellar oxygen chemistry.

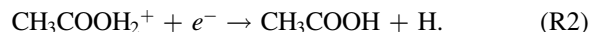
Key words: astrochemistry – cosmic rays – ISM: molecules – methods: laboratory: solid state – molecular processes – radiation mechanisms: non-thermal

1. Introduction

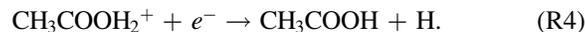
In recent years, considerable attention from experimental physical chemists to observational astrophysicists has been devoted to untangling the formation routes of three structural isomers of C₂H₄O₂: acetic acid (CH₃COOH), methyl formate (HCOOCH₃), and glycolaldehyde (HCOCH₂OH) (Bennett & Kaiser 2007a, 2007b; Kim & Kaiser 2010; Puletti et al. 2010; Shiao et al. 2010; Guan et al. 2012; Burke et al. 2014; Favre et al. 2017; Zhu et al. 2018a) (Figure 1). Among these structural isomers—molecules with the same chemical formula but distinct connectivity of the atoms—acetic acid (CH₃COOH) is considered as a critical prebiotic molecule, since it shares the C–C=O(OH) backbone with the simplest amino acid glycine (NH₂CH₂COOH), from which acetic acid differs only by an amino group (–NH₂).

The first detection of acetic acid in the interstellar medium (ISM) was made toward Sgr B2(N-LMH) (Mehring et al. 1997) with a column density of 6.1 × 10¹⁵ cm^{−2} and a relative abundance to molecular hydrogen of (3.4 ± 2.6) × 10^{−10}. Subsequent detections were made toward low- and high-mass star-forming regions such as W51e2 (Remijan et al. 2002), G19.61–0.23 (Shiao et al. 2010), IRAS 16293–2422 (Jørgensen et al. 2016), and the Orion-KL nebula (Favre et al. 2017). In these objects the column density of CH₃COOH was determined to be a few × 10¹⁶ cm^{−2}, with an estimated relative abundance to hydrogen of 1.7 × 10^{−9} in W51e2 (Remijan et al. 2002). Acetic acid was also detected in the solar system by the *Rosetta* mission on the surface of the comet 67P/Churyumov–Gerasimenko (Altwegg et al. 2017). Additionally, an upper limit of acetic acid of 0.06% compared to water was proposed for the comet C/1996 O1 (Hale–Bopp; Crovisier et al. 2004). However, despite

these astronomical observations, the underlying formation pathways of acetic acid (CH₃COOH) in the ISM have still remained unclear. Gas phase and grain surface chemistry alone are insufficient to match observations (Garrod et al. 2008; Bergantini et al. 2017). Initially, Huntress & Mitchell (1979) proposed a radiative association mechanism via reaction (R1) followed by an unstudied dissociative recombination with an electron (R2):



Alternatively, an experimentally unstudied transfer of an alkyl cation from protonated methanol to formic acid (HCOOH) (R3) followed by a dissociative recombination to acetic acid (R4) was proposed by Ehrenfreund & Charnley (2000):



Gas-phase studies suggested that acetic acid may be formed via the reaction of the acetyl and hydroxyl radicals (R5) or through reactions between the hydroxycarbonyl and methyl radicals (R6) (Fang et al. 2002):



However, bimolecular reactions in the gas phase cannot divert the internal excess energy gained via C–O bond formation, and acetic acid will rather dissociate back owing to the lack of any third-body dissociation. Additionally, there are several factors that indicate that gas-phase reactions alone are not enough to

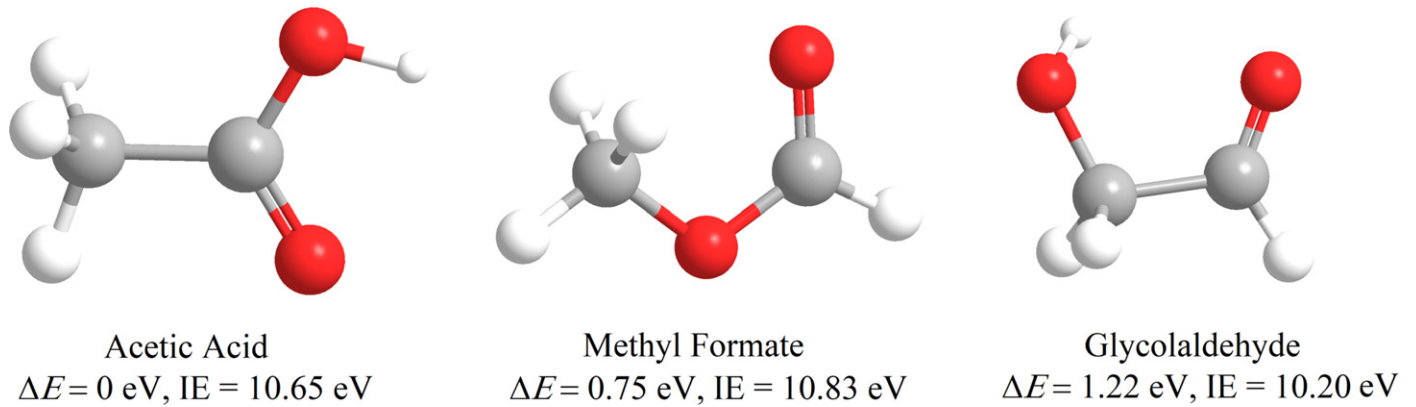


Figure 1. Molecular structures, relative energies (ΔE), and ionization energies (IEs) of $C_2H_4O_2$ isomers acetic acid (CH_3COOH), methyl formate ($HCOOCH_3$), and glycolaldehyde ($HCOCH_2OH$).

account for the formation of acetic acid in these environments. For example, the gas-phase-only model of Wlodarczak & Demaison (1988) predicts a relative abundance of acetic acid in Sgr B2 of 2×10^{-11} , which is up to two orders of magnitude lower than the observations (Remijan et al. 2002). Additionally, the temperature and velocity of acetic acid in Sgr B2 are characteristic of that of species thought to be formed within icy grains (Mehringer et al. 1997; Remijan et al. 2002), suggesting that the formation of acetic acid in the ISM is associated with processes that occur inside interstellar ice grains, most likely due to the interaction between ice grains and energetic particles such as cosmic rays, as evidenced in numerous studies (Kaiser & Roessler 1998; Bisschop et al. 2007a; Bayet et al. 2011; Mason et al. 2014). Therefore, the primary objective of the present study is to evaluate—using single photoionization (PI) coupled with a reflectron time-of-flight mass spectrometer (ReTOF-MS)—to what extent acetic acid can be formed *inside* ices containing carbon dioxide (CO_2) and methane (CH_4) when exposed to energetic electrons, mimicking the processing of nonpolar interstellar ices by secondary particles released in the track of galactic cosmic rays, as they penetrate interstellar ice grains (Kaiser & Roessler 1997, 1998; Bennett et al. 2005a; Alizadeh et al. 2015).

Both CO_2 and CH_4 have been recognized as components of interstellar ices and of frozen solar system objects. Data from the *Infrared Space Observatory* (ISO) revealed that CO_2 is a ubiquitous component of dust grain ices found inside dust-embedded young stellar objects (YSOs; Cook et al. 2011), where the CO_2 abundance relative to solid H_2O reaches levels above 40% in sources such as L1489 IR, IRAS 04154+2823, Elias 18, CG 12, IRS 63, and R CrA IRS5 (Tanaka et al. 1994; Chiar et al. 1998; Pontoppidan et al. 2003, 2008; Cook et al. 2011). The detection of CH_4 in molecular clouds and toward YSOs has been repeatedly substantiated as well (Boogert et al. 1996). Methane was first reported toward the objects NGC 7538 IRS 9, OMC-1 IRc2, and W33A (Lacy et al. 1991), and significant CH_4 detections were made toward objects such as SVS 4–5, L1014 IRS, IRAS 03235+3004, and L1489 IRS (Graninger et al. 2016) and toward the sources L1455 SMM 1, IRAS 15398–3359, IRS 42, IRS 43, IRS 63, GSS 30, VSSG 17, and CrA IRAS 32 (Öberg et al. 2008). In these objects, the relative abundance of CH_4 can reach levels of up to 8% and 11%, respectively. Moreover, models and observations predict that CO_2 and CH_4 (as well as H_2O and CH_3OH) are formed

very early in protostellar regions through linked and similar processes (Gerakines et al. 1999; Boogert et al. 2000; Knez et al. 2005; Öberg et al. 2008). Considering that laboratory data strongly suggest that these small species are the fundamental building blocks of complex organic molecules (COMs), ice mixtures containing some combination of CO_2 , CH_4 , H_2O , and/or CH_3OH are often used to model the chemistry of the early stages of evolution of molecular clouds, especially when the intention is to determine the feasibility of particular reaction pathways of species of interest. For this reason, the carbon dioxide–methane (CO_2 – CH_4) mixture was chosen in this study to evaluate the proof of concept that acetic acid, as well as acetic acid dimers, can be produced in apolar ices, under anhydrous conditions, via interaction with ionizing radiation.

It is important to notice that previous laboratory investigations have shown that dissimilar ice mixtures can lead to comparable qualitative results, proving that the formation of complex organic species heavily relies on key precursors, which can be synthesized in ice mixtures with different compositions, granted that all the base elements are present (Öberg et al. 2010; Bergantini et al. 2017, 2018b). Therefore, it is possible to determine the feasibility of formation pathways of astrophysical species of interest using simplified model ices, even if the quantitative results may not be comparable with the processes that occur in the ISM.

Laboratory investigations by Bennett & Kaiser (2007a), Kim & Kaiser (2010), and Zhu et al. (2018a) have shown that the formation of carboxylic acid functional groups (including acetic acid) might be possible. However, the assignment of the products in these studies was carried out based on infrared features and functional groups, which could be associated with a variety of carboxylic acids owing to overlapping bands. This represents the most significant drawback of Fourier transform infrared spectroscopy (FTIR) compared to PI-ReTOF-MS, as the latter is able to selectively identify *individual* isomers based on their distinct ionization energies (IEs; Bergantini et al. 2017, 2018b; Förstel et al. 2017; Abplanalp et al. 2018a, 2018b). Since PI-ReTOF-MS is extremely sensitive, low-dose experiments at doses as low as $0.88 \pm 0.12 \text{ eV}$ per molecule of carbon dioxide and $0.32 \pm 0.04 \text{ eV}$ per molecule of methane (Table 1) can be performed, which is equivalent to the dose deposited by cosmic rays inside typical molecular clouds in a mere $(2.0 \pm 0.5) \times 10^6 \text{ yr}$ (Yeghikyan 2011). Such low-dose experiments provide fundamental data and mechanistical

Table 1
Data Applied in the Calculation of the Average Dose per
Molecule in the Irradiated Ices

Initial kinetic energy of the electrons, E_{init} (keV) ^a	5
Irradiation current, I (nA) ^a	19 ± 1
Total number of electrons ^a	$(1.1 \pm 0.3) \times 10^{14}$
Average penetration depth, l (nm) ^a	358 ± 16
Maximum penetration depth (nm) ^a	560 ± 50
Average kinetic energy of backscattered electrons, E_{bs} (keV) ^a	3.43 ± 0.21
Fraction of backscattered electrons, f_{bs} ^a	0.40 ± 0.04
Average kinetic energy of transmitted elec- trons, E_{trans} (keV) ^a	0
Fraction of transmitted electrons, f_{trans} ^a	0
Density of the ice, ρ (g cm ⁻³)	0.85 ± 0.04
Irradiated area, A (cm ²)	1.0 ± 0.1
Dose (eV/molecule):	
Carbon dioxide	0.88 ± 0.12
Methane	0.32 ± 0.04

Note.

^a Parameters obtained from CASINO software v2.42.

information on the *initial steps* involved in the formation of carboxylic acids without successive reaction of the latter.

2. Experimental

The experiments were carried out in a stainless steel ultrahigh-vacuum chamber (UHV) evacuated to a base pressure of a few $\times 10^{-11}$ torr. Ice mixtures were prepared via deposition of premixed gases onto a polished silver substrate coupled to a cold finger, cooled at temperatures of 5.5 ± 0.2 K using a closed-cycle helium cryostat (Sumitomo Heavy Industries, RDK-415E). The compounds used in the experiment—carbon dioxide (CO₂, 99.999%, BOC gases; C¹⁸O₂, 97% atom ¹⁸O, Sigma-Aldrich) and methane (CH₄, 99.999%, Specialty Gases of America; CD₄, Aldrich, 99% + atom D)—were premixed in a gas mixing chamber (GMC) kept at pressures of a few $\times 10^{-8}$ torr otherwise. The partial pressures of carbon dioxide and methane in the GMC prior to the deposition were 100.0 ± 0.1 torr and 10.0 ± 0.1 torr, respectively. Three experiments using distinct gas mixtures (CO₂-CH₄, CO₂-CD₄, and C¹⁸O₂-CH₄) were performed in this work. The gaseous samples were deposited by a glass capillary array. The pressures in the main chamber were kept at $(2.0 \pm 0.2) \times 10^{-8}$ torr for 600 ± 20 s during depositing of the molecules. The ice growth was monitored online and in situ by measuring the interference pattern (fringes) produced by a 632.8 nm HeNe laser (CVI Melles Griot; 25-LHP-230) as the laser beam was reflected off the silver substrate into a photodiode interfaced to a picoammeter (Keithley 6485). The ice thickness (650 ± 20 nm) was measured using the methodology described by Bergantini et al. (2017) and Turner et al. (2015), exploiting a refractive index for the mixture of 1.22 ± 0.03 (Luna et al. 2012). According to Monte Carlo simulations performed by the CASINO software (v2.42; Drouin et al. 2007), the thickness of 650 ± 20 nm is sufficient to ensure minimal interaction between the impinging electrons and the substrate, since the maximum penetration depth of the electrons was determined to be 560 ± 50 nm (Table 1). In these calculations we have adopted a density of 0.85 ± 0.04 g cm⁻³ for the CO₂-CH₄ (16:1) ice based on the work of Luna et al. (2012).

The ratio of carbon dioxide to methane in the unirradiated ices was calculated based on the column density of each reactant measured by FTIR with the support of the methodology described by Turner et al. (2016). The areas of the IR peaks used were the $\nu_1 + \nu_3$ band of carbon dioxide (3708 cm⁻¹) and the ν_3 band of methane (3010 cm⁻¹). The absorption coefficients adopted were taken from Bouilloud et al. (2015) and correspond to 1.8×10^{-18} cm molecule⁻¹ for the $\nu_1 + \nu_3$ band of carbon dioxide and 1.1×10^{-18} cm molecule⁻¹ for the ν_3 band of methane, which yielded to a CO₂-CH₄ ratio in the unirradiated ices of (16 ± 1) to 1.

The ice samples were monitored by an electron-impact quadrupole mass spectrometer (IE-QMS; Extrel 5221) operating in residual gas analyzer mode (RGA) and by FTIR spectroscopy (Nicolet 6700) before and during the irradiation and by RGA and PI-ReTOF-MS during the temperature programmed desorption (TPD) after the irradiation. The irradiation was carried out using 5 keV electrons at a current of (19 ± 1) nA for 15 minutes, at an angle of 70° relative to the surface normal of the substrate. Based on CASINO simulations (Drouin et al. 2007), the irradiation yields to a dose of 0.88 ± 0.12 eV per molecule of carbon dioxide and 0.32 ± 0.04 eV per molecule of methane (Table 1).

After the irradiation, the sample was kept isothermally at 5.5 ± 0.2 K for 1 hr until the beginning of the TPD. In the TPD phase the sample was warmed up to 300 K at a rate of 1 K minute⁻¹, when vacuum ultraviolet (VUV) photons were exploited to softly ionize the molecules as they desorbed from the ice into the gas phase. In the present experiments, VUV light with energy of 10.84 eV (114.38 nm) was used. This pulsed (30 Hz) coherent VUV light was generated using resonant four-wave difference mixing ($\omega_{\text{VUV}} = 2\omega_1 - \omega_2$). In this process, the ω_1 light is generated by pumping 532 nm (2.33 eV) photons from a neodymium-doped yttrium aluminum garnet (Nd:YAG) laser (Spectra Physics, PRO-270-30), which is then converted to 606.94 nm (2.04 eV) using a dye laser (Sirah Lasertechnik, Cobra-Stretch), before frequency tripling the output of the dye laser using a pair of β -BaB₂O₄ (BBO) crystals (angles of 44° and 77°), which generates 202.31 nm (6.13 eV) photons. The ω_2 light is generated by pumping 532 nm photons from another Nd:YAG laser (Spectra Physics, PRO-250-30), which is then converted to 875.30 nm (1.41 eV) using a second dye laser (Sirah Lasertechnik, Precision Scan). Both beams (ω_1 and ω_2) are overlapped into a differentially pumped vacuum chamber where pulsed jets of krypton (99.999%; Specialty Gases) are used as a nonlinear medium to produce the 10.84 eV photons through the process of resonant four-wave-mixing ($\omega_{\text{VUV}} = 2\omega_1 - \omega_2$). Finally, the VUV light is passed through a 1 mm aperture before reaching the subliming molecules from the ice sample at 1 mm above the surface of the substrate. The flux of VUV photons at 10.84 eV was measured by a photodiode calibrated by the National Institute of Standards and Technology (NIST), and the average flux corresponds to $(3.5 \pm 0.5) \times 10^{11}$ photons s⁻¹. The ions generated from the interaction with the VUV photons were detected and mass-resolved by ReTOF-MS (Jordan TOF Products, Inc.) using a multichannel plate in a dual chevron configuration. The signal was then amplified by a fast preamplifier (Ortec 9305) and shaped with a 100 MHz discriminator. The resulting spectrum was recorded by a personal-computer-based multichannel scalar (FAST ComTec, P7888-1 E) with a bin width of 4 ns, triggered at 30 Hz by a

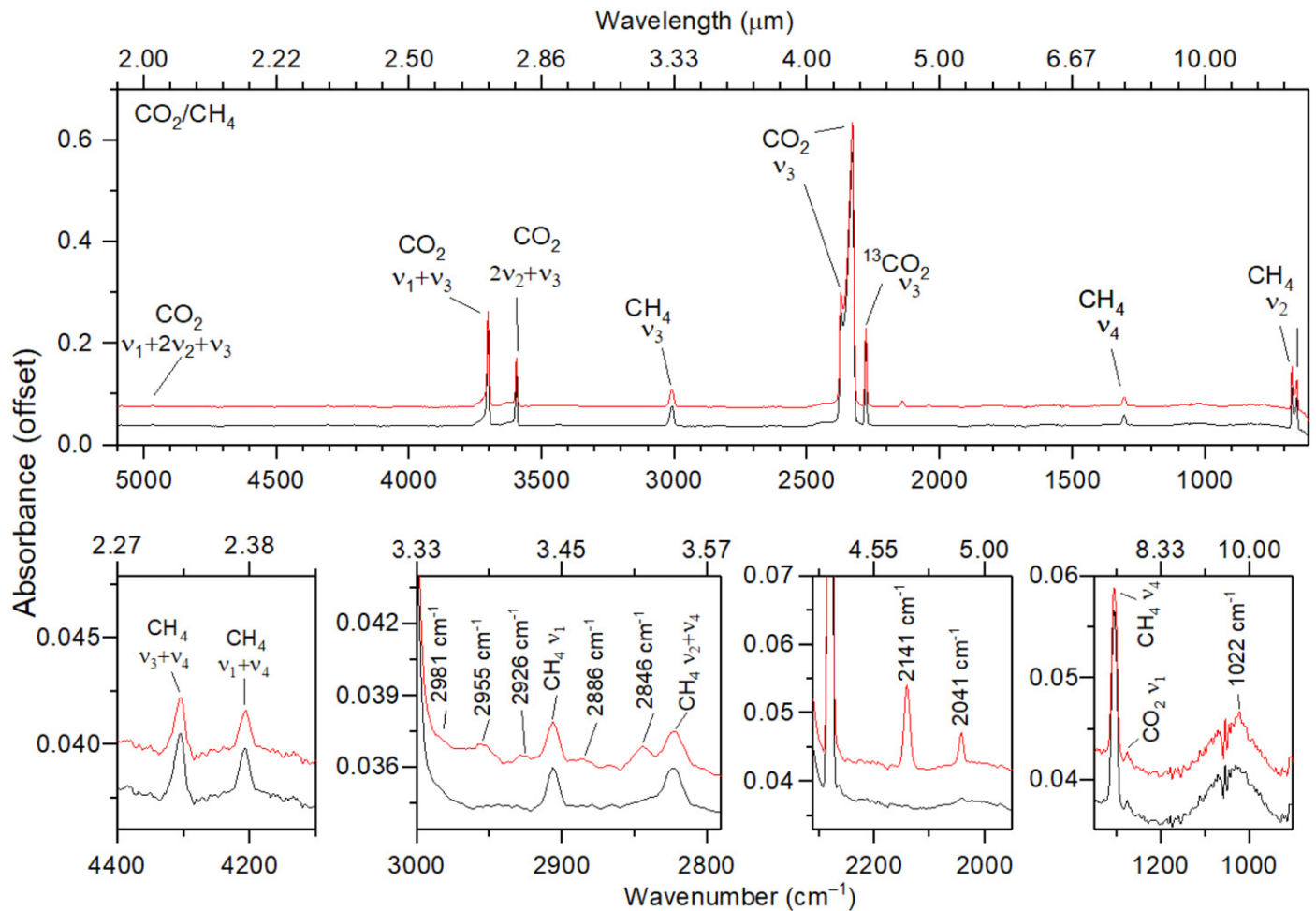


Figure 2. Infrared spectra of carbon dioxide (CO₂)–methane (CH₄) ices before (black trace) and after (red trace) the irradiation.

signal generator (Quantum Composers, 9518). The ReTOF-MS produces 3600 sweeps per mass spectrum every 2 minutes.

3. Results and Discussion

3.1. FTIR

First, we present the FTIR bands detected before and after the irradiation of the carbon dioxide–methane ices. Figure 2 displays the infrared spectra of the CO₂–CH₄ sample recorded at 5.5 K before (black trace) and after (red trace) the irradiation. Likewise, Figures 3 and 4 show the infrared spectra of the isotopically labeled mixture of carbon dioxide and D₄-methane (CO₂–CD₄) and of ¹⁸O carbon dioxide and methane (C¹⁸O₂–CH₄), respectively, before (black trace) and after (red trace) the irradiation. The infrared features of the samples are compiled in Table 2 (unirradiated ice) and in Table 3 (irradiated ice), in ascending order of wavenumber. The analysis of the results reveals that the new species produced within the ices are methanol (CH₃OH), detected at 1022 cm⁻¹ in the CO₂–CH₄ sample and at 995 cm⁻¹ in the C¹⁸O₂–CH₄ sample; carbon trioxide (CO₃), observed at 2043 cm⁻¹ in the CO₂–CH₄ and CO₂–CD₄ samples and at 2006 cm⁻¹ in the C¹⁸O₂–CH₄ sample (Bennett et al. 2010); carbon monoxide (CO), monitored via the ν₁ mode observed at 2141 cm⁻¹ in the CO₂–CH₄ and CO₂–CD₄ ices and at 2090 cm⁻¹ in the C¹⁸O₂–CH₄ ice; and ethane (C₂H₆), observed at 2846 cm⁻¹ in the CH₄–CO₂

experiment and at 2843 cm⁻¹ in the CH₄/C¹⁸O₂ experiment (Hepp & Herman 1999; Abplanalp et al. 2018a). Note that no significant shift in position of the C₂H₆ band in the CH₄–CO₂ experiment was observed in comparison with the CH₄–C¹⁸O₂ sample, which suggests that this feature belongs to an oxygenless species, which also applies for the bands detected at 2886, 2074, and 2887 cm⁻¹. Even though the assignment of the bands detected at 2926 and 2955 cm⁻¹ in the CO₂–CH₄ experiment is not conclusive, we conclude that these bands belong to –CH₂– and –CH₃ asymmetric stretch modes (Socrates 2004); additionally, the 2981 cm⁻¹ band was assigned to the ν₁₀ mode of ethane (C₂H₆) (Abplanalp et al. 2018a); finally, the peaks at 3523 (CO₂–CH₄ ice), 2683, 2605 (CO₂–CD₄ ice), and 3381 cm⁻¹ (C¹⁸O₂–CH₄ ice) were assigned to O–H/O–D stretches of acid monomers (Socrates 2004).

3.2. PI-ReTOF-MS—Acetic Acid

After irradiation, the samples were slowly warmed up so that the sublimating products could be probed by PI-ReTOF-MS at a photon energy of 10.84 eV, so any species that has IE of up to 10.84 eV can be ionized and detected by the spectrometer. This process was supported by the use of combinations of isotopically labeled reactants, so the unique mass shifts of the ions could be exploited to determine the molecular formulae of

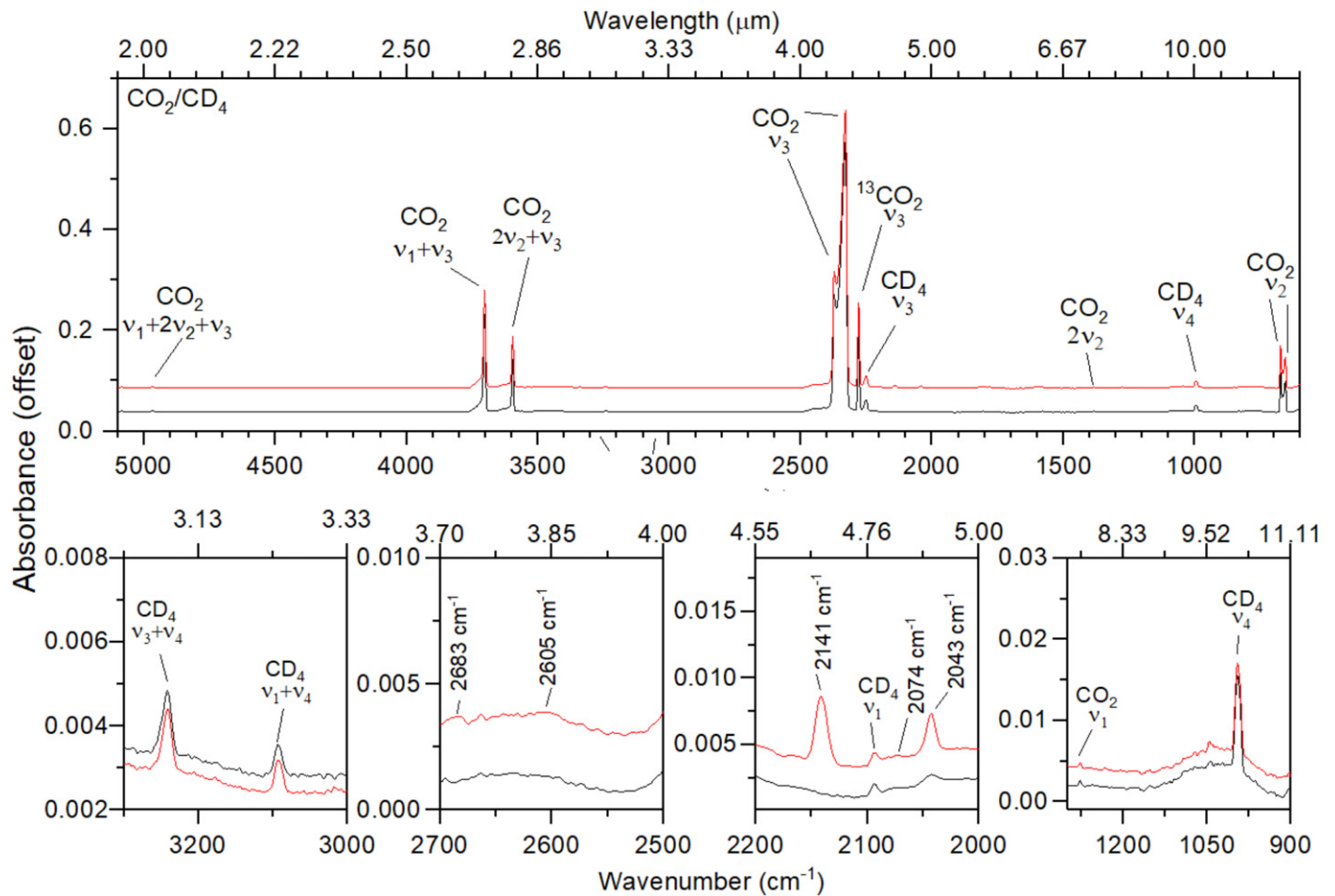


Figure 3. Infrared spectra of carbon dioxide (CO₂)-D₄-methane (CD₄) ices before (black trace) and after (red trace) the irradiation.

the products. The PI-ReTOF-MS data recorded as a function of temperature from all three experiments are compiled in Figure 5, which shows mass-to-charge ratios of up to 125 in the 5–300 K temperature interval. Most importantly, the detailed analysis of the data depicted in Figure 5 reveals the detection of acetic acid monomers and dimers, among more COMs of astrophysical interest, as discussed below.

Since we are interested in investigating the formation of acetic acid (CH₃COOH) inside CO₂-CH₄ ices, we begin the analysis by observing the TPD profile at a mass-to-charge ratio of 60 ($m/z = 60$; Figure 6), as two distinct groups of isomers might contribute to this signal: species with general formula C₂H₄O₂ and the ones with formula C₃H₈O. To determine whether the signal at $m/z = 60$ is from C₂H₄O₂ or C₃H₈O isomers (or both), we have exploited isotopic substitution experiments using ¹⁸O and D labeling, which would shift the potential mass-to-charge signals from C₂H₄O₂ isotopomers by 4 amu, whereas the signal of C₃H₈O isotopomers would shift by 2 and 8 amu owing to ¹⁸O and D labeling, respectively. Consequently, PI-ReTOF-MS signals from C₂H₄O₂ isotopomers would be found at $m/z = 60$ and 64, whereas C₃H₈O peaks would be found at $m/z = 60$, 62, and 68. As Figure 6(b) reveals, no signals from C₃D₈O and C₃H₈¹⁸O were detected in our experiments, implying that only C₂H₄O₂ isomers contribute to the signal at $m/z = 60$ in the CO₂-CH₄ experiment (Figure 6(a)). Therefore, the potential C₂H₄O₂ isomers detected in our experiments are acetic acid (CH₃COOH, IE = 10.65 eV), methyl formate (HCOOCH₃, IE = 10.835 eV),

glycolaldehyde (HOCH₂CHO, IE = 10.20 eV), and ethen-1,2-diol (HOCHCHOH, IE = 9.62 eV).

In principle, since the IE of all C₂H₄O₂ isomers is below the photoionization energy of 10.84 eV used in the present experiments, the specific assignment of the signal at $m/z = 60$ to one species in particular would not be possible. However, laboratory studies have revealed that gas-phase acetic acid (CH₃COOH) forms a strongly bound dimer (CH₃COOH)₂ involving two hydrogen bonds (Forysinski et al. 2011; Guan et al. 2012), while the hydrogen bonding in the trimer (CH₃COOH)₃ was shown to be less favorable. Using supersonic beams of acetic acid monomers, dimers, and trimers, coupled to tunable vacuum ultraviolet light, to detect and count the resulting ions, Guan et al. (2012), Hu et al. (2006), and Zielke et al. (2009) revealed that upon soft photoionization ionized acetic acid dimers and trimers undergo reaction and fragment in a pattern characterized by signal from acetic acid (CH₃COOH⁺) ($m/z = 60$), by protonated clusters ((CH₃COOH)_{*n*}·H⁺) ($m/z = 61$ [$n = 1$], 121 [$n = 2$], 181 [$n = 3$]), and by cluster fragments ((CH₃COOH)_{*n*}·CH₃CO⁺) ($m/z = 103$ [$n = 2$], 163 [$n = 3$]) and ((CH₃COOH)_{*n*}·COOH⁺) ($m/z = 105$ [$n = 2$], 165 [$n = 3$]). Therefore, in the following section we will search for these ions to trace potential acetic acid clusters. Also, it should be stressed that these ion counts are unique to clusters of acetic acid, but not to methyl formate, glycolaldehyde, or ethen-1,2-diol. Consequently, the detection of acetic acid can be made based on the signal from the acetic acid ion CH₃COOH⁺ ($m/z = 60$) and

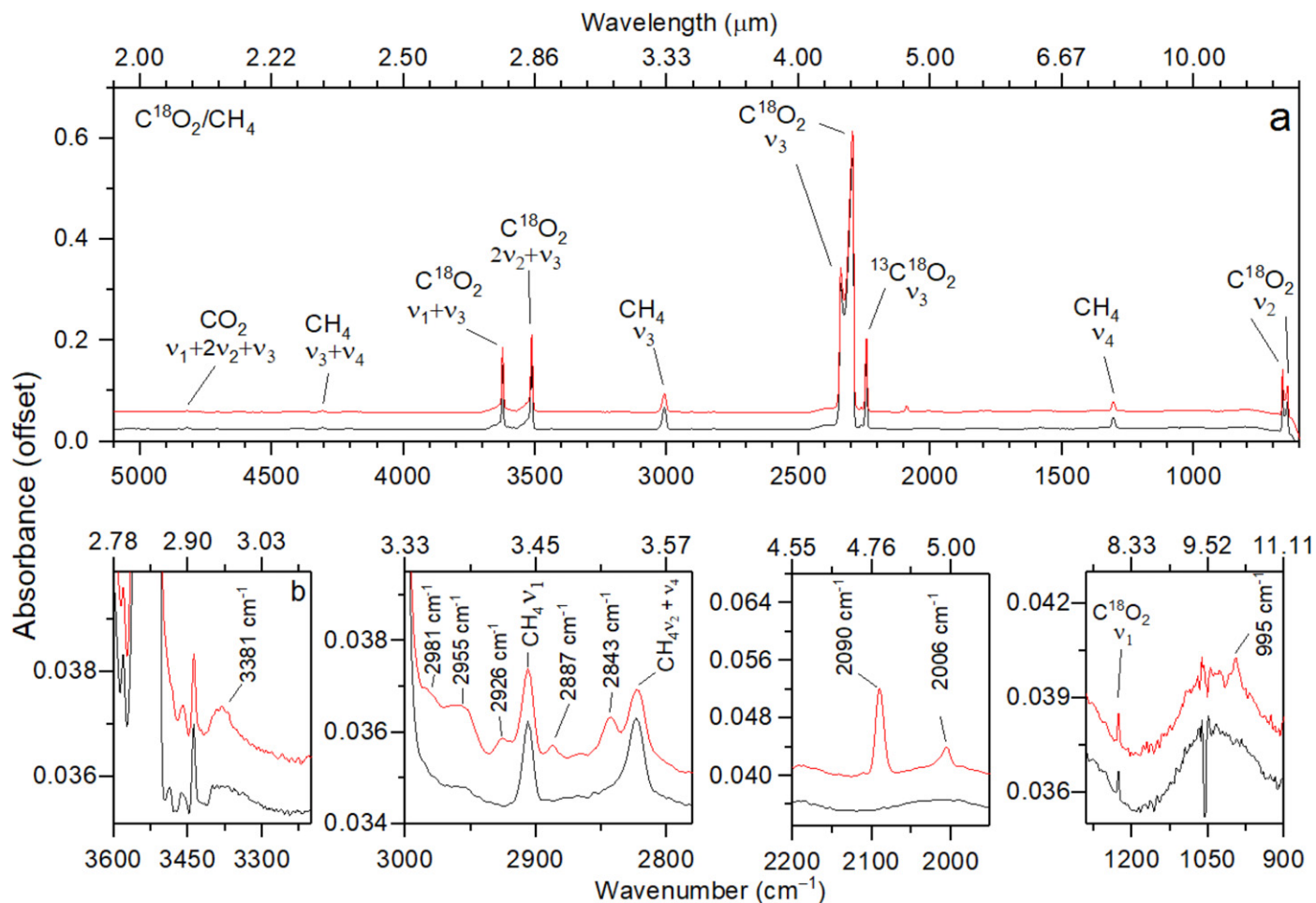


Figure 4. Infrared spectra of carbon dioxide ($C^{18}O_2$)–methane (CH_4) ices before (black trace) and after (red trace) the irradiation.

from two fragments of the dimer: $(CH_3COOH) \cdot H^+$ ($m/z = 61$) and $(CH_3COOH) \cdot COOH^+$ ($m/z = 105$), as will be demonstrated. Fragments of trimers were not detected either because of the relatively low conversion of carbon dioxide–methane to acetic acid or because the energy used to photoionize the subliming molecules in our experiments is insufficient to produce trimer fragments such as $(CH_3COOH) \cdot CH_3CO^+$ ($m/z = 103$), which has an appearance energy of 12.41 eV (Guan et al. 2012).

Let us then analyze the acetic acid monomer, dimer, and trimer signals—or lack thereof—as compiled in Figure 7. We already established that $m/z = 60$ (Figure 7(a)) belongs to $C_2H_4O_2$ isomers, and among them is acetic acid. The signal at $m/z = 61$ ($(CH_3COOH)H^+$; Figure 7(b)) represents the most common fragment of acetic acid dimers (Hu et al. 2006; Zielke et al. 2009; Forsynski et al. 2011; Guan et al. 2012), with the $(CH_3COOH) \cdot COOH^+$ fragment detected at $m/z = 105$ (Figure 7(c)) being the second most intense (Hu et al. 2006; Zielke et al. 2009; Forsynski et al. 2011). Notably, the signals from the isotopologues of $(CH_3COOH)H^+$ and $(CH_3COOH) \cdot COOH^+$ were also confirmed (Figures 7(b) and (c)), thus supporting the detection of acetic acid dimers. In principle, the fragment $(CH_3COOH) \cdot CH_3CO^+$, which originates from the acetic acid trimer (Forsynski et al. 2011), would be detected at $m/z = 103$, but its appearance energy is above the energy of 10.84 eV used in our experiments. Therefore, the signal seen in the middle row of Figure 7(d) (CO_2 – CD_4 ice)

at $m/z = 110$ must originate from the dimer fragment $(CD_3COOD) \cdot COOD^+$ (Figure 7(c)). Finally, Figure 7(e) reveals that the signal from $(CH_3COOH)_2 \cdot H^+$ ($m/z = 121$), a fragment of the acetic acid trimer, is not observed in any of our experiments, despite the fact that such a fragment is commonly detected in gas-phase studies on the photoionization of neat samples of acetic acid (Hu et al. 2006; Zielke et al. 2009; Guan et al. 2012). This could be explained by the concentration of acetic acid in our samples, which could be too low to allow the formation of trimers. Therefore, based on these considerations, we conclude that our experiments have successfully identified acetic acid dimer along with the isotopically substituted counterparts in our samples.

Besides the isotopic labeling study, the detection of acetic acid can be supported by comparing the TPD profile of $m/z = 61$ from our work with calibration experiments, in which neat samples are deposited and warmed up without any processing. For instance, Burke et al. (2014) collected TPD profiles of neat samples of methyl formate ($HCOOCH_3$), glycolaldehyde ($HOCH_2CHO$), and acetic acid (CH_3COOH). These studies revealed that acetic acid sublimates within the 144 ± 2 K to 171 ± 2 K temperature interval, which is consistent with the sublimation profile of $m/z = 61$ ($(CH_3COOH)H^+$) observed in our experiments. This configures as another evidence that the signal at $m/z = 61$ belongs to protonated acetic acid, which, in turn, implies that the signal at

Table 2
Infrared Absorptions of the Methane and Carbon Dioxide Ice Mixtures Along with the Assignments of the Observed Bands

Band Position (cm ⁻¹)			Assignment	Characterization
CO ₂ /CH ₄	CO ₂ /CD ₄	C ¹⁸ O ₂ /CH ₄		
5085	5085	4970	CO ₂ /C ¹⁸ O ₂ (2ν ₁ + ν ₃)	Combination
4967	4967	4822	CO ₂ /C ¹⁸ O ₂ (ν ₁ + 2ν ₂ + ν ₃)	Combination
4829	4829	4707	CO ₂ /C ¹⁸ O ₂ (4ν ₂ + ν ₃)	Combination
4305	4478	4305	CH ₄ /CD ₄ (ν ₃ + ν ₄)	Combination
4207	4574	4207	CH ₄ /CD ₄ (ν ₁ + ν ₄)	Combination
3703	3703	3623	CO ₂ /C ¹⁸ O ₂ (ν ₁ + ν ₃)	Combination
3596	3596	3515	CO ₂ /C ¹⁸ O ₂ (2ν ₂ + ν ₃)	Combination
3010	2251	3010	CH ₄ /CD ₄ (ν ₃)	Fundamental
2906	2095	2906	CH ₄ /CD ₄ (ν ₁)	Fundamental
2823	3092	2823	CH ₄ (ν ₂ + ν ₄)	Combination
2374, 2330	2374, 2330	2341, 2296	CO ₂ /C ¹⁸ O ₂ (ν ₃)	Fundamental
2279	2279	2243	¹³ CO ₂ / ¹³ C ¹⁸ O ₂ (ν ₃)	Fundamental
1384	1384	1338	CO ₂ /C ¹⁸ O ₂ (2ν ₂)	Overtone
1277	1277	1227	CO ₂ /C ¹⁸ O ₂ (ν ₁)	Fundamental
1307	995	1307	CH ₄ /CD ₄ (ν ₄)	Fundamental
673, 655	673, 655	663, 643	CO ₂ /C ¹⁸ O ₂ (ν ₂)	Fundamental

$m/z = 60$ (Figure 7(a)) has the contribution of acetic acid. Moreover, the results observed by Burke et al. (2014) show that glycolaldehyde (HOCH₂CHO) is detected in the 140–160 K interval, which is also consistent with the TPD profile at $m/z = 60$ from our experiments (Figure 6(a)). This means that we may have also detected HOCH₂CHO in our experiments, since glycolaldehyde (HOCH₂CHO) can be easily formed in astrophysical ices in which methanol and carbon monoxide—two species that were in fact detected in our experiments (Table 3, Figure 4)—are found as neighboring molecules (Bennett & Kaiser 2007b). Finally, further investigation of the TPD profiles reveals no signs of methyl formate (HCOOCH₃), the third C₂H₄O₂ isomer, as this species sublimates at approximately 100 K, when there is no positive detection in any of our experiments.

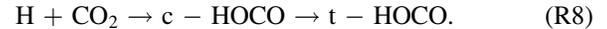
The nondetection of methyl formate from processed CO₂–CH₄ ices agrees with the results of Bennett & Kaiser (2007a, 2007b), which concluded that this species can be readily produced in a process involving the methoxy (CH₃O) and formyl (HCO) radicals, which are common products in methanol–carbon monoxide ices exposed to ionizing radiation. In our experiments, however, theoretical and experimental data from the literature (Song et al. 2006; Bennett & Kaiser 2007a, 2007b; Zhu et al. 2018b) reveal that the cause for methyl formate not being formed in our experiments—at least in measurable amounts—is probably the fact that an important precursor, the formyloxyl (HCOO) radical, is less stable than the cis/trans-hydroxycarbonyl (HOCO) radicals (Song et al. 2006) formed in our ices. Therefore, the pathway to acetic acid (see reaction R8 below) is preferred over methyl formate. A similar conclusion was recently drawn by Zhu et al. (2018b) on the synthesis of H₂PCOOH (phosphino formic acid) in CO₂-bearing ices.

In summary, our results are in agreement with the results obtained by Bennett & Kaiser (2007a) and Zhu et al. (2018a) after a comprehensive kinetic modeling on the formation of carboxylic acids in CO₂–CH₄ ices. They have established that acetic acid is formed in the solid phase *inside the ices* first via the decomposition of methane, via cleavage of a carbon–hydrogen bond, to form the methyl radical plus hydrogen

(reaction R7), which is endoergic by 427 kJ mol⁻¹ (4.4 eV):



The hydrogen released in reaction (R7) holds an excess of energy of a few eV; therefore, it can add to the carbon dioxide molecule, thus forming the trans-carboxyl radical (t-HOCO), which requires the intermediate step to the cis conformer (c-HOCO) (Song et al. 2006; Bennett & Kaiser 2007a):



Finally, acetic acid can be formed barrierlessly via the recombination of methyl radical (CH₃) and carboxyl radical (HOCO), if they are both formed inside the matrix cage with the correct geometry to recombination:



Reaction (R9) is exoergic by 365 kJ mol⁻¹ (3.78 eV; Nguyen et al. 1995; Bennett & Kaiser 2007a). However, the energetics point out that nonequilibrium chemistry triggered by cosmic rays is necessary to start the pathway to the formation of the acetic acid in astrophysical CO₂–CH₄-rich grains.

3.3. PI-ReTOF-MS—Additional Species

3.3.1. $m/z = 44$

Besides the detection of acetic acid monomers and dimers, additional assignments were also made based on the PI-ReTOF-MS data. The signal corresponding to $m/z = 44$ in the CO₂–CH₄ experiment can potentially be assigned to C₂H₄O isomers (Figure 8(a)) and/or to propane (C₃H₈) (Figure 8(b)). Figure 8(a) shows that the signal at $m/z = 44$ is in good agreement with the TPD profiles of $m/z = 48$ from the CO₂–CD₄ experiment and with $m/z = 46$ from the C¹⁸O₂–CH₄ experiment, therefore indicating the presence of C₂H₄O based on the mass shifts upon isotopic substitution. Since no signal is present at $m/z = 44$ (C₃D₈⁺) in the CO₂–CD₄ experiment, we conclude that $m/z = 44$ cannot contain eight deuterium atoms, thus proposing the absence of propane (C₃H₈). Consequently, signal at $m/z = 44$ can be assigned to C₂H₄O isomers acetaldehyde (CH₃CHO; IE = 10.22 eV),

Table 3
New Absorption Peaks Observed in CH₄/CO₂, CD₄/CO₂, and CH₄/C¹⁸O₂ Ice after the Irradiation

Wavenumber (cm ⁻¹)			Assignment	Carrier	References
CO ₂ /CH ₄	CO ₂ /CD ₄	C ¹⁸ O ₂ /CH ₄			
3523	2683, 2605	3381	acid monomers	O–H stretch	Socrates (2004)
2981	...	2981	ν_{10} C ₂ H ₆	CH ₃ stretch	Shimanouchi (1972)
2955	...	2955	...	–CH ₃ asym. stretch	Socrates (2004)
2926	...	2926	...	–CH ₂ –asym. stretch	Socrates (2004)
2886	2074	2887	ν_5 C ₂ H ₆	–CH ₃ sym. stretch	Bennett et al. (2006)
2846	...	2843	$\nu_2 + \nu_4 + \nu_{12}$ C ₂ H ₆	combination	Hepp & Herman (1999)
2141	2141	2090	ν_1 CO	C–O/C– ¹⁸ O stretch	Kim & Kaiser (2010)
2043	2043	2006	C ₂ , ν_1 CO ₃	C=O/ C= ¹⁸ O ₃ stretch	Moll et al. (1966)
1022	...	995	ν_8 CH ₃ OH	C–O stretch	Bergantini et al. (2014)

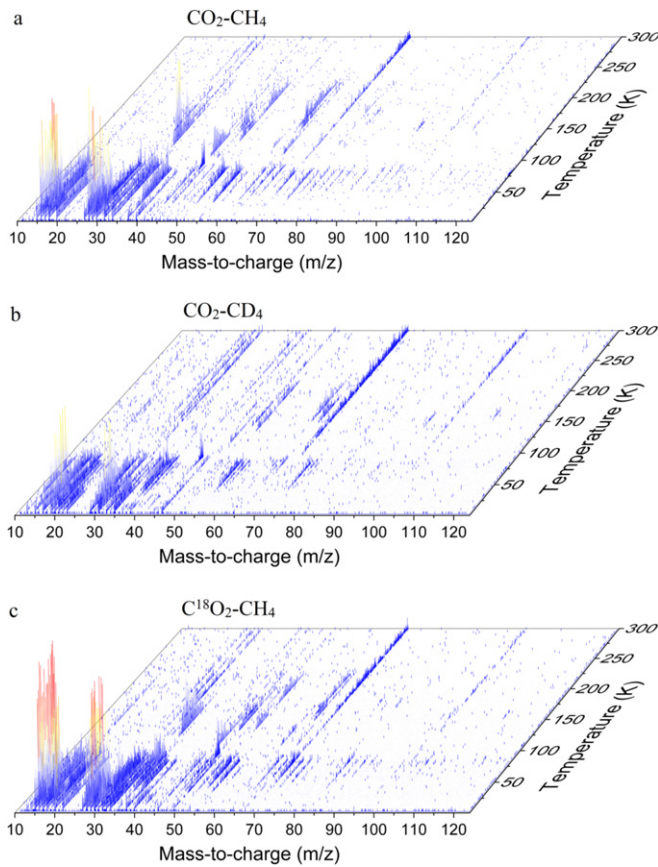


Figure 5. PI-ReTOF-MS data reporting the temperature-dependent mass spectra at a photoionization energy of 10.84 eV for irradiated (a) CO₂–CH₄, (b) CO₂–CD₄, and (c) C¹⁸O₂–CH₄ ices.

ethylene oxide (c-C₂H₄O; IE = 10.56 eV), and/or vinyl alcohol (CH₂CHOH; IE = 9.33 eV). Note that acetaldehyde (CH₃CHO) and vinyl alcohol (CH₂CHOH) were detected by Abplanalp et al. (2016) in electron-irradiated methane (CH₄)–carbon monoxide (CO) ices. Since carbon monoxide was in fact also detected in our experiments, the synthesis of acetaldehyde (CH₃CHO) from the processing of CO₂–CH₄ seems to be feasible. Likewise, methane can be easily converted to ethylene (C₂H₄) (Kaiser & Roessler 1998; Bennett et al. 2006; Jones & Kaiser 2013; Kaiser et al. 2014; Abplanalp et al. 2018a), which may react with suprathreshold oxygen atoms to form ethylene oxide (c-C₂H₄O) (Bennett et al. 2005b).

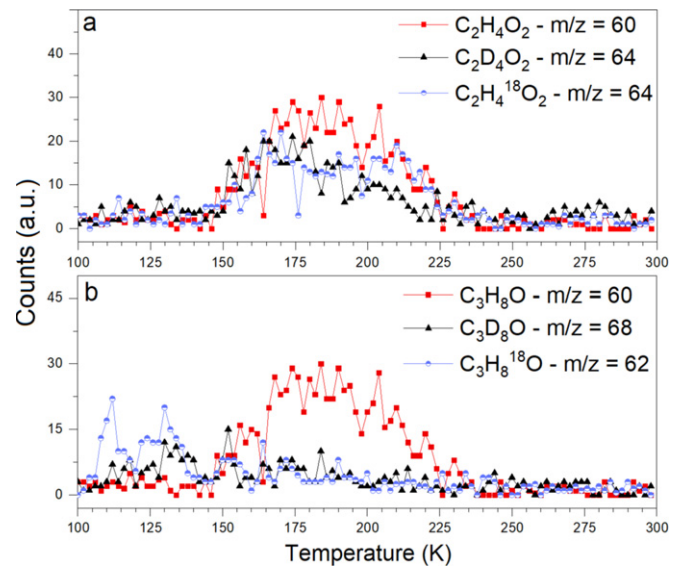


Figure 6. TPD profiles of species detected at $m/z = 60$, which may include C₂H₄O₂ and C₃H₈O isomers. The comparison of the data collected from the isotopically labeled experiments reveals that the signal detected at $m/z = 60$ belongs to C₂H₄O₂ isomers (Figure 6(a)), but not to C₃H₈O isomers (Figure 6(b)).

3.3.2. $m/z = 46$

The signal from $m/z = 46$ (Figure 8(c)) can be associated only with ethanol (CH₃CH₂OH, IE = 10.48 eV) and dimethyl ether (CH₃OCH₃, IE = 10.02 eV), as the IE of formic acid (HCOOH; 11.33 eV) is above the energy of 10.84 eV used in the experiments. The corresponding TPD profiles of C₂D₆O⁺ and C₂H₆ ¹⁸O⁺ are observed at $m/z = 52$ in the CO₂–CD₄ experiment and at $m/z = 48$ in the C¹⁸O₂–CH₄ system, respectively, confirming the detection of C₂H₆O isomers. The formation of ethanol and dimethyl ether in astrophysical model ices was extensively studied by Bergantini et al. (2017, 2018b), which linked the formation of ethanol and dimethyl ether to the presence of methanol in the ice. Finally, note that the signal at $m/z = 52$ in the CO₂–CD₄ experiment reveals a second sublimation event between 175 and 220 K. This sublimation event is associated with CD₄O₂ (see Section 3.3.3).

3.3.3. $m/z = 48$

Signal at $m/z = 48$ (Figure 8(d)) can be potentially assigned to ozone (O₃), methyl hydroperoxide (CH₃OOH), and methanediol (methylene glycol, CH₂(OH)₂). The mass shifts

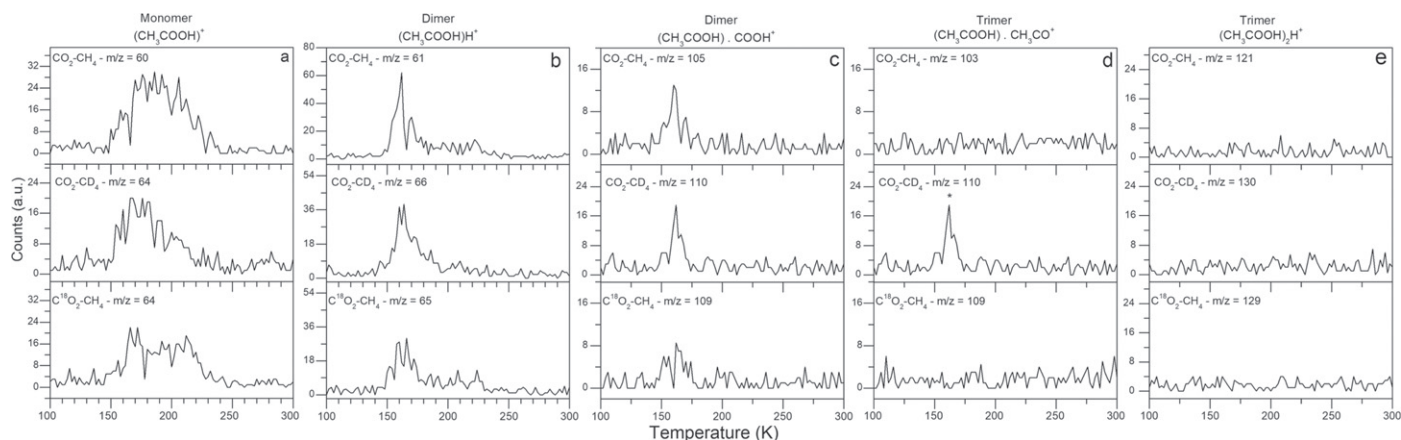


Figure 7. TPD profiles of ion signal connected to acetic acid (CH_3COOH) and its clusters synthesized in the $\text{CO}_2\text{-CH}_4$ (top row), $\text{CO}_2\text{-CD}_4$ (middle row), and $\text{C}^{18}\text{O}_2\text{-CH}_4$ (bottom row) ices. Since the ionization energy of $(\text{CD}_3\text{COOD})\text{-CD}_3\text{CO}^+$ is above the energy used in the experiments, the signal in the middle row of panel (d) must belong to $(\text{CD}_3\text{COOD})\text{-COOD}^+$. Also, note that the dip at 164 ± 1 K in the first row of panels (a)–(c) was caused by a momentary loss of the VUV signal from the laser beams.

in the $\text{CO}_2\text{-CD}_4$ and $\text{C}^{18}\text{O}_2\text{-CH}_4$ experiments confirm the detection of CH_2O_2 isomers. On the other hand, since the IE of ozone of 12.53 eV is above the photon energy used in the present experiments, the detection of such species is discarded. Although methanediol is believed to be present in the ISM (Ehrenfreund & Charnley 2000), it was experimentally found to eliminate water (H_2O) prior to sublimation upon annealing thus reacting to formaldehyde (H_2CO). Therefore, signal at $m/z = 48$ cannot be linked to methanediol in our system. Methyl hydroperoxide (CH_3OOH), the simplest organic peroxide, could be produced via methane oxidation essentially via the recombination of methoxy radicals (CH_3O) with hydroxyl radicals (OH).

3.3.4. $m/z = 58$

There are three groups of isomers associated with $m/z = 58$: C_4H_{10} , $\text{C}_2\text{H}_2\text{O}_2$, and $\text{C}_3\text{H}_6\text{O}$. Once again, isotopic shifts can be exploited to assist in the identification. The examination of Figures 8(e)–(g)—which shows the comparison between the signals from all the possible isotopomers mentioned above—reveals that the best match is achieved when comparing the signals from C_4H_{10} and C_4D_{10} , even though the signals are weak. Note from Figure 8(f) that the signal from $\text{C}_2\text{D}_2\text{O}_2$ (glyoxal) is absent and the corresponding signals from the $\text{CO}_2\text{-CH}_4$ and $\text{C}^{18}\text{O}_2\text{-CH}_4$ experiments do not match, confirming that glyoxal ($\text{C}_2\text{H}_2\text{O}_2$) is not detected. Finally, Figure 8(g) excludes the possibility of detection of $\text{C}_3\text{H}_6\text{O}$ isomers, which would include important COMs such as acetone, propanal, and propylene oxide—the first chiral molecule detected in the ISM (McGuire et al. 2016; Bergantini et al. 2018a). The two possible C_4H_{10} isomers detected are *i*-butane (IE = 10.68 eV) and *n*-butane (IE = 10.53 eV), species not yet observed in the ISM but recently detected by Abplanalp et al. (2018a) upon irradiation of pure methane ices. Here butane (C_4H_{10}) is suggested to be formed by the recombination of two ethyl radicals (C_2H_5), which, in turn, are generated from radiolysis of ethane (C_2H_6). In our system, ethane is formed via carbene (CH_2) insertion in a carbon–hydrogen bond of methane (CH_4) or recombination of two methyl radicals (Hudson et al. 2009; Kim et al. 2010; Abplanalp & Kaiser 2016).

3.3.5. $m/z = 74$

Candidates for weak signal at $m/z = 74$ are the isomers $\text{C}_3\text{H}_6\text{O}_2$ (Figure 8(h)), $\text{C}_2\text{H}_2\text{O}_3$ (Figure 8(i)), and $\text{C}_4\text{H}_{10}\text{O}$ (Figure 8(j)). As Figure 8(h) reveals, based on the isotopic shifts, there is a good agreement between the signal of $\text{C}_3\text{H}_6\text{O}_2$ and its isotopologues. The possible $\text{C}_3\text{H}_6\text{O}_2$ isomers are propanoic acid ($\text{C}_2\text{H}_5\text{COOH}$, IE = 10.44 eV), methyl acetate ($\text{CH}_3\text{COOCH}_3$, IE = 10.25 eV), ethyl formate (HCOOC_2H_5 , IE = 10.61 eV), 1-hydroxypropan-2-one (hydroxyacetone, $\text{CH}_3\text{C}(\text{O})\text{CH}_2\text{OH}$, IE = 10.0 eV), dioxolane (IE = 9.9 eV), glycidol (IE = 10.43 eV), and methoxyacetaldehyde. Among these species, methyl acetate and ethyl formate were detected in Orion-KL (Tercero et al. 2013).

4. Astrophysical Implications and Conclusions

Our research demonstrated that acetic acid can be readily produced in ice mixtures of carbon dioxide (CO_2) and methane (CH_4) subject to irradiation by energetic electrons produced by the interaction between cosmic rays and interstellar grains. Similarly, acetic acid could be formed in ices inside cold molecular clouds and in ice-covered dust grains found in regions of star formation, through nonequilibrium reactions triggered by cosmic rays, with the formation of clusters of acetic acid (CH_3COOH) following the sublimation of the ice in the vicinity of a protostar, as the temperature rises. Further, exploiting *extremely* low irradiation in our experiments does provide outstanding information regarding chemistry of the early stages of evolution of molecular clouds. For instance, by exposing $\text{CO}_2\text{-CH}_4$ ices with doses more than two orders of magnitude higher than in our work, Zhu et al. (2018a) detected complex carboxylic acids ($\text{C}_n\text{H}_{2n+1}\text{COOH}$, $n < 10$), which were not detected in our study. These differences can be easily explained by the level of processing of the samples, which in turn increases the level of complexity of the organic molecules formed in the processed ices. Beyond the acetic acid detection, we would like to bring attention to the astrophysical implications concerning some of the signals detected in our work.

Unlike similar studies involving the processing of methane ices (Kaiser & Roessler 1998; Yeghikyan et al. 2001; Jones & Kaiser 2013; Abplanalp et al. 2018a; Zhu et al. 2018a), no high-mass hydrocarbons were detected in our investigation. In

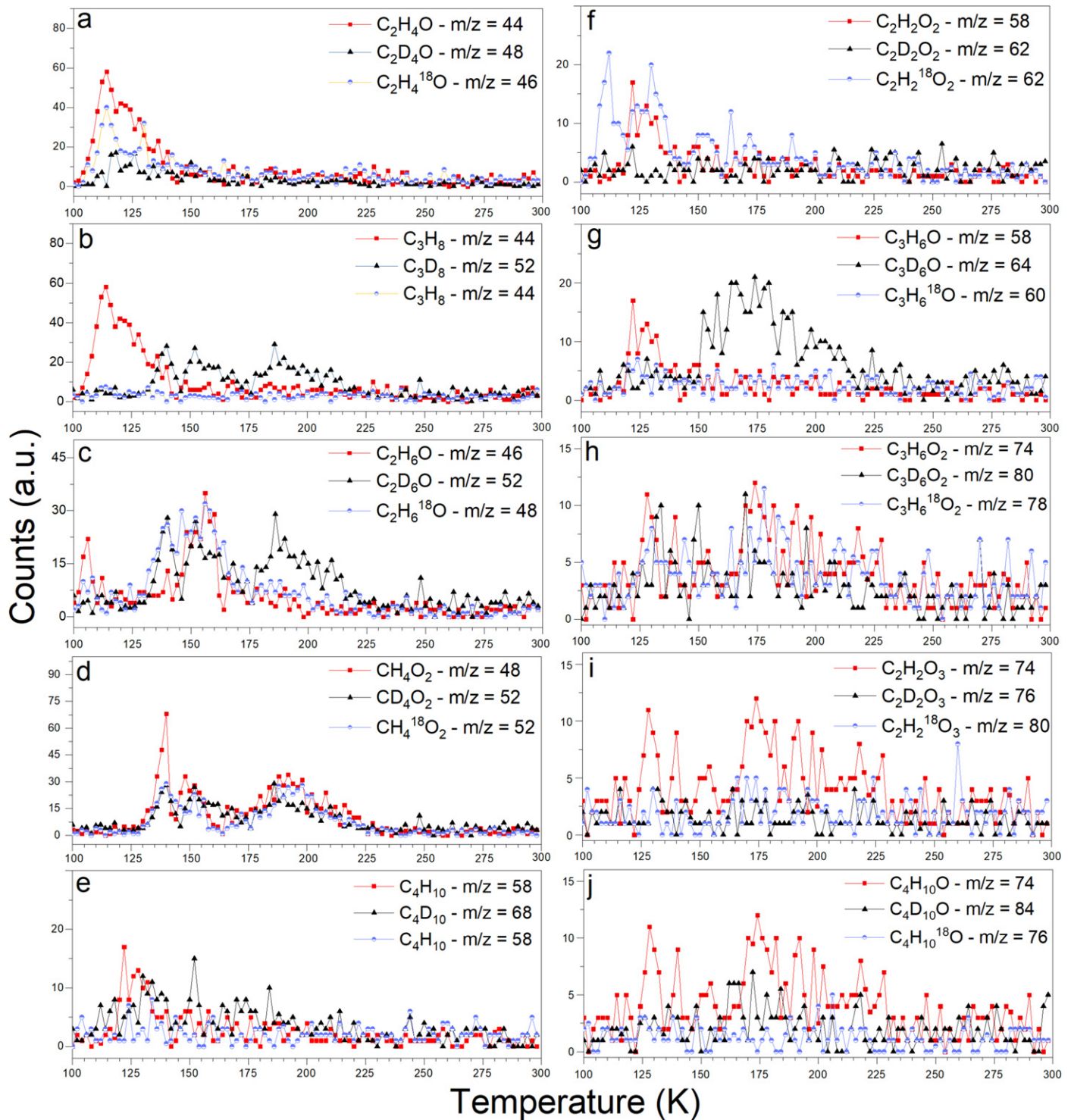


Figure 8. TPD profiles of distinct mass-to-charge ratios recorded in the $\text{CO}_2\text{-CH}_4$ (red squares), $\text{CO}_2\text{-CD}_4$ (black triangles), and $\text{C}^{18}\text{O}_2\text{-CH}_4$ experiments (blue circles).

fact, the only hydrocarbons detected were C_4H_{10} (PI-ReTOF-MS, Figure 8(e)) and C_2H_6 (FTIR, Table 3). Since hydrocarbons are expected to be swiftly produced as methane is exposed to ionizing irradiation, the lack of heavier hydrocarbons is likely the consequence of the low dose of irradiation. Some of the species detected in our experiments are commonly found in star-forming regions. That is the case of $\text{C}_2\text{H}_4\text{O}$ isomers (Figure 8(a)), which could be vinyl alcohol (CH_2CHOH), acetaldehyde (CH_3CHO), and/or ethylene oxide ($\text{c-C}_2\text{H}_4\text{O}$).

Vinyl alcohol was detected in Sgr B2 (Turner & Apponi 2001); acetaldehyde was found in high-mass star-forming regions, such as Sgr B2 and Orion-KL (Gottlieb 1973; Turner 1991), and in the low-mass star-forming region HH 212 (hot corino) in Orion (Codella et al. 2016); and ethylene oxide was observed in Sgr B2(N) (Dickens et al. 1997). The $\text{C}_2\text{H}_6\text{O}$ isomers, ethanol ($\text{CH}_3\text{CH}_2\text{OH}$) and dimethyl ether (CH_3OCH_3) (Figure 8(c)), were both detected in the Orion Nebula (Snyder et al. 1974; Pearson et al. 1997), toward the high-mass star-forming regions

NGC 6334 IRS1, G24.78, W3(H₂O), W33A (Bisschop et al. 2007b), W51e2, G34.3+0.2 (Lykke et al. 2015), G31.41+0.31 (Rivilla et al. 2017), and Orion-KL (White et al. 2003; Crockett et al. 2014), in low-mass star-forming regions NGC 1333 IRAS 2A and IRAS 4A (Taquet et al. 2015), and in multiple sources toward the Galactic center, including Sgr B2(N) (Requena-Torres et al. 2006). The signal at $m/z = 48$ (Figure 8(d)) is likely to be from methyl hydroperoxide (CH₃OOH), a molecule that can be formed by the oxidation of methane (Epstein et al. 2012), but that has not been detected in the ISM yet. Among the C₃H₆O₂ isomers detected in our work (Figure 8(h)) are ethyl formate (C₂H₅OCHO), found in Sgr B2(N) (Belloche et al. 2009) and in Orion-KL (Tercero et al. 2013), and methyl acetate (CH₃COOCH₃), also found in Orion-KL (Tercero et al. 2013). These isomer-specific differences can be used as references in the interpretation of astronomical observations, as certain isomers can be used as tracers of chemical and physical conditions, as demonstrated by Bergantini et al. (2017) and Turner et al. (2015).

In conclusion, in this work we have positively identified via PI-ReTOF-MS acetic acid monomers and dimers—among them additional organic species relevant to astronomy—in processed ices of carbon dioxide and methane. The deposited dose of irradiation in our samples is one or two orders of magnitude lower than what is found in most studies involving the processing of analog ices at $T < 10$ K, and the results found here point to a question that deserves to be investigated more deeply on how different are the qualitative results following “high”- and “low”-dose experiments involving astrophysical model ices, as it may have implications for the early evolutionary stages of molecular clouds. In conclusion, we suggest that two elusive species, acetic acid dimer (CH₃COOH)₂ and methyl hydroperoxide (CH₃OOH), are outstanding candidates to be detected in regions of star formation, given how facile is the formation of such species inside astrophysical model CO₂–CH₄ ices even at doses of irradiation that correspond to only the very first stages of evolution of a typical molecular cloud. Finally, since Bergantini et al. (2018b) have detected the also yet astrophysically elusive dimethyl peroxide (CH₃OOCH₃) in processed methanol–methane (CH₃OH–CH₄) ices, we conclude that methyl hydroperoxide and dimethyl peroxide are likely present in the ISM, thus completing the homologous series of peroxides HOOH (Bergman et al. 2011), CH₃OOH, and CH₃OOCH₃.

We thank the US National Science Foundation (AST-1505502) for support in conducting the present experiments. The authors would like to acknowledge the W. M. Keck Foundation for financing the experimental setup.

ORCID iDs

Alexandre Bergantini  <https://orcid.org/0000-0003-2279-166X>

Cheng Zhu  <https://orcid.org/0000-0002-7256-672X>

Ralf I. Kaiser  <https://orcid.org/0000-0002-7233-7206>

References

- Abplanalp, M., Jones, B., & Kaiser, R. I. 2018a, *PCCP*, **20**, 5435
- Abplanalp, M. J., Góbi, S., Bergantini, A., Turner, A. M., & Kaiser, R. I. 2018b, *Chem Phys Chem*, **19**, 556
- Abplanalp, M. J., Gozem, S., Krylov, A. I., et al. 2016, *PNAS*, **113**, 7727
- Abplanalp, M. J., & Kaiser, R. I. 2016, *ApJ*, **827**, 132
- Alizadeh, E., Orlando, T. M., & Sanche, L. 2015, *ARPC*, **66**, 379
- Altwegg, K., Balsiger, H., Berthelier, J. J., et al. 2017, *MNRAS*, **469**, S130
- Bayet, E., Williams, D. A., Hartquist, T. W., & Viti, S. 2011, *MNRAS*, **414**, 1583
- Belloche, A., Garrod, R. T., Müller, H. S. P., et al. 2009, *A&A*, **499**, 215
- Bennett, C. J., Jamieson, C. S., & Kaiser, R. I. 2010, *PCCP*, **12**, 4032
- Bennett, C. J., Jamieson, C. S., Osamura, Y., & Kaiser, R. I. 2005a, *ApJ*, **624**, 1097
- Bennett, C. J., Jamieson, C. S., Osamura, Y., & Kaiser, R. I. 2006, *ApJ*, **653**, 792
- Bennett, C. J., & Kaiser, R. I. 2007a, *ApJ*, **660**, 1289
- Bennett, C. J., & Kaiser, R. I. 2007b, *ApJ*, **661**, 899
- Bennett, C. J., Osamura, Y., Lebar, M. D., & Kaiser, R. I. 2005b, *ApJ*, **634**, 698
- Bergantini, A., Abplanalp, M. J., Pokhilko, P., et al. 2018a, *ApJ*, **860**, 108
- Bergantini, A., Góbi, S., Abplanalp, M. J., & Kaiser, R. I. 2018b, *ApJ*, **852**, 70
- Bergantini, A., Maksyutenko, P., & Kaiser, R. I. 2017, *ApJ*, **841**, 1
- Bergantini, A., Nair, B. G., Mason, N. J., & Fraser, H. J. 2014, *A&A*, **570**, A120
- Bergman, P., Parise, B., Liseau, R., et al. 2011, *A&A*, **531**, L8
- Bisschop, S. E., Fuchs, G. W., van Dishoeck, E. F., & Linnartz, H. 2007a, *A&A*, **474**, 1061
- Bisschop, S. E., Jørgensen, J. K., Van Dishoeck, E. F., & De Wachter, E. B. M. 2007b, *A&A*, **465**, 913
- Boogert, A. C. A., Schutte, W. A., Tielens, A. G. G. M., et al. 1996, *A&A*, **315**, L377
- Boogert, A. C. A., Tielens, A. G. G. M., Ceccarelli, C., et al. 2000, *A&A*, **360**, 683
- Bouilloud, M., Fray, N., Bénilan, Y., et al. 2015, *MNRAS*, **451**, 2145
- Burke, D. J., Puletti, F., Brown, W. A., et al. 2014, *MNRAS*, **447**, 1444
- Chiar, J. E., Gerakines, P. A., Whittet, D. C. B., et al. 1998, *ApJ*, **498**, 716
- Codella, C., Ceccarelli, C., Cabrit, S., et al. 2016, *A&A*, **586**, L3
- Cook, A. M., Whittet, D. C. B., Shenoy, S. S., et al. 2011, *ApJ*, **730**, 124
- Crockett, N. R., Bergin, E. A., Neill, J. L., et al. 2014, *ApJ*, **787**, 112
- Crovisier, J., Bockelée-Morvan, D., Colom, P., et al. 2004, *A&A*, **418**, 1141
- Dickens, J. E., Irvine, W. M., Ohishi, M., et al. 1997, *ApJ*, **489**, 753
- Drouin, D., Couture, A. R., Joly, D., et al. 2007, *Scanning*, **29**, 92
- Ehrenfreund, P., & Charnley, S. B. 2000, *ARA&A*, **38**, 427
- Epstein, S. A., Shemesh, D., Tran, V. T., Nizkorodov, S. A., & Gerber, R. B. 2012, *JPCA*, **116**, 6068
- Fang, W.-H., Liu, R.-Z., Zheng, X., & Phillips, D. L. 2002, *JORG*, **67**, 8407
- Favre, C., Pagani, L., Goldsmith, P., et al. 2017, *A&A*, **604**, L2
- Förstel, M., Bergantini, A., Maksyutenko, P., Góbi, S., & Kaiser, R. I. 2017, *ApJ*, **845**, 83
- Forysinski, P. W., Zielke, P., Luckhaus, D., Corbett, J., & Signorell, R. 2011, *JChPh*, **134**, 094314
- Garrod, R. T., Weaver, S. L. W., & Herbst, E. 2008, *ApJ*, **682**, 283
- Gerakines, P. A., Whittet, D. C. B., Ehrenfreund, P., et al. 1999, *ApJ*, **522**, 357
- Gottlieb, C. A. 1973, in *Molecules in the Galactic Environment*, ed. M. A. Gordon & L. E. Snyder (New York: John Wiley and Sons), 181
- Graninger, D. M., Wilkins, O. H., & Öberg, K. I. 2016, *ApJ*, **819**, 140
- Guan, J., Hu, Y., Zou, H., et al. 2012, *JChPh*, **137**, 124308
- Hepp, M., & Herman, M. 1999, *JMoSp*, **197**, 56
- Hu, Y., Fu, H., & Bernstein, E. 2006, *JChPh*, **125**, 184308
- Hudson, R. L., Moore, M. H., & Raines, L. L. 2009, *Icar*, **203**, 677
- Huntress, W., Jr. & Mitchell, G. 1979, *ApJ*, **231**, 456
- Jones, B. M., & Kaiser, R. I. 2013, *J Phys Chem Lett*, **4**, 1965
- Jørgensen, J. K., Van der Wiel, M. H. D., Coutens, A., et al. 2016, *A&A*, **595**, A117
- Kaiser, R. I., Maity, S., & Jones, B. M. 2014, *PCCP*, **16**, 3399
- Kaiser, R. I., & Roessler, K. 1997, *ApJ*, **475**, 144
- Kaiser, R. I., & Roessler, K. 1998, *ApJ*, **503**, 959
- Kim, Y. S., Bennett, C. J., Chen, L.-H., O’Brien, K., & Kaiser, R. I. 2010, *ApJ*, **711**, 744
- Kim, Y. S., & Kaiser, R. I. 2010, *ApJ*, **725**, 1002
- Knez, C., Boogert, A. C. A., Pontoppidan, K. M., et al. 2005, *ApJL*, **635**, L145
- Lacy, J., Carr, J., Evans, N. J., et al. 1991, *ApJ*, **376**, 556
- Luna, R., Satorre, M., Domingo, M., Millán, C., & Santonja, C. 2012, *Icar*, **221**, 186
- Lykke, J. M., Favre, C., Bergin, E. A., & Jørgensen, J. K. 2015, *A&A*, **582**, A64
- Mason, N. J., Nair, B., Jheeta, S., & Szymańska, E. 2014, *FaDi*, **168**, 235
- McGuire, B. A., Carroll, P. B., Loomis, R. A., et al. 2016, *Sci*, **352**, 1449
- Mehring, D. M., Snyder, L. E., Miao, Y., & Lovas, F. J. 1997, *ApJL*, **480**, L71
- Moll, N. G., Clutter, D. R., & Thompson, W. E. 1966, *JChPh*, **45**, 4469

- Nguyen, M. T., Sengupta, D., Raspoet, G., & Vanquickenborne, L. G. 1995, *JPhCh*, 99, 11883
- Öberg, K. I., Boogert, A. C. A., Pontoppidan, K. M., et al. 2008, *ApJ*, 678, 1032
- Öberg, K. I., Van Dishoeck, E. F., Linnartz, H., & Andersson, S. 2010, *ApJ*, 718, 832
- Pearson, J. C., Sastry, K. V. L. N., Herbst, E., & De Lucia, F. C. 1997, *ApJ*, 480, 420
- Pontoppidan, K. M., Boogert, A. C., Fraser, H. J., et al. 2008, *ApJ*, 678, 1005
- Pontoppidan, K. M., Fraser, H. J., Dartois, E., et al. 2003, *A&A*, 408, 981
- Puletti, F., Mallocci, G., Mulas, G., & Cecchi-Pestellini, C. 2010, *MNRAS*, 402, 1667
- Remijan, A., Snyder, L. E., Liu, S.-Y., Mehringer, D., & Kuan, Y.-J. 2002, *ApJ*, 576, 264
- Requena-Torres, M. A., Martín-Pintado, J., Rodríguez-Franco, A., et al. 2006, *A&A*, 455, 971
- Rivilla, V. M., Beltrán, M. T., Cesaroni, R., et al. 2017, *A&A*, 598, A59
- Shiao, Y.-S. J., Looney, L. W., Remijan, A. J., Snyder, L. E., & Friedel, D. N. 2010, *ApJ*, 716, 286
- Shimanouchi, T. 1972, *JPCRD*, 1, 189
- Snyder, L. E., Buhl, D., Schwartz, P. R., et al. 1974, *ApJL*, 191, L79
- Socrates, G. 2004, *Infrared and Raman Characteristic Group Frequencies: Tables and Charts* (New York: Wiley)
- Song, X., Li, J., Hou, H., & Wang, B. 2006, *JChPh*, 125, 094301
- Tanaka, M., Nagata, T., Sato, S., & Yamamoto, T. 1994, *ApJ*, 430, 779
- Taquet, V., López-Sepulcre, A., Ceccarelli, C., et al. 2015, *ApJ*, 804, 81
- Tercero, B., Kleiner, I., Cernicharo, J., et al. 2013, *ApJL*, 770, L13
- Turner, A. M., Abplanalp, M. J., Chen, S. Y., et al. 2015, *PCCP*, 17, 27281
- Turner, A. M., Abplanalp, M. J., & Kaiser, R. I. 2016, *ApJ*, 819, 97
- Turner, B. E. 1991, *ApJS*, 76, 617
- Turner, B. E., & Apponi, A. J. 2001, *ApJL*, 561, L207
- White, G. J., Araki, M., Greaves, J. S., Ohishi, M., & Higginbottom, N. S. 2003, *A&A*, 407, 589
- Włodarczak, G., & Demaison, J. 1988, *A&A*, 192, 313
- Yeghikyan, A. 2011, *Ap*, 54, 87
- Yeghikyan, A. G., Viti, S., & Williams, D. A. 2001, *MNRAS*, 326, 313
- Zhu, C., Frigge, R., Turner, A. M., et al. 2018b, *ChCom*, 54, 5716
- Zhu, C., Turner, A. M., Abplanalp, M. J., & Kaiser, R. I. 2018a, *ApJS*, 234, 1
- Zielke, P., Forysinski, P. W., Luckhaus, D., & Signorell, R. 2009, *JChPh*, 130, 211101